NJC

New Journal of Chemistry

A journal for new directions in chemistry

Accepted Manuscript

This article can be cited before page numbers have been issued, to do this please use: L. Tom, C. R. Nirmal, A. D. V. N., M. Balasubramanian and M. R. P. Kurup, *New J. Chem.*, 2020, DOI: 10.1039/C9NJ06351J.

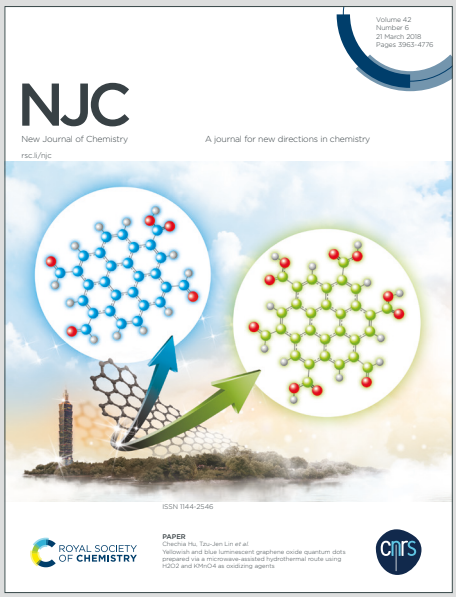

View Article Online
DOI: 10.1039/C9NJ06351J

ARTICLE

Formulation and Evaluation of β-Cyclodextrin-mediated Inclusion Complexes of Isoniazid Scaffolds: Molecular Docking and *In Vitro* Assessment of Antitubercular Properties

Received 00th January 20xx,
Accepted 00th January 20xx

DOI: 10.1039/x0xx00000x

Lincy Tom[a*], Christy Rosaline Nirmal[b], Azger Dusthackeer[b], B. Mahizhaveni[b] and M.R. P. Kurup[c]

Poor aqueous solubility is the major problem encountered with formulation of new bioactive chemical entities. In the present study, we report the synthesis and evaluation of inclusion complexes between two poorly water soluble antitubercular agents (*p*-hydroxybenzaldehydeisonicotinylhydrazone (HBIH) and 2,3-butanedionebisisonicotinylhydrazone (BDIH)) and *β*-cyclodextrin. Solubility of these compounds has been enhanced by inclusion complexation and the solid complexes were characterized using FTIR, PXRD, NMR and SEM. Phase-solubility studies indicated that HBIH/BDIH formed a 1:1 stoichiometric inclusion complex with *β*-CD. Moreover, molecular docking analysis identified the most favorable host-guest interactions in the inclusion complexes. The complexes were evaluated against *Mycobacterium tuberculosis* strains and exhibited more than 95% growth inhibition. The complexes were devoid of cytotoxicity when tested against L929 fibroblast cell lines. Docking studies were carried out on DprE1 and Thymidine Monophosphate Kinase protein enzymes to provide some understanding into the mechanism of action of these compounds.

1. Introduction

Mycobacterium tuberculosis (Mtb), an infectious bacillus, is the causative agent of many cases of tuberculosis and is the deadliest communicable disease prevalent in all parts of the world.[1] Epidemiological studies have indicated that 10 million people, as much as one third of the world's population, are infected by tuberculosis every year.[2] Mycobacteria can evade the host immune system and remain dormant for a long period of time. This allows the Mtb to reactivate to a virulent form under immune-compromised conditions of the host.[3] The enduring persistence of Mtb in dormant stage helps the pathogen to establish resistance against current anti-mycobacterial drugs.[4] Almost all of the antibiotics that can be used to treat TB work when the bacteria are actively dividing. However, in order to kill the persistent or slow growing strains of Mtb, the continuation phase of the treatment is essential. Thus, there is an urgent need for the development of new drugs and strategies which can tackle the dormant Mtb and for the eradication of the disease.

TB can be effectively treated with first-line drugs isoniazid, pyrazinamide, rifampin and streptomycin.[5-8] However, this first-line therapy often fails to cure the TB due to the emergence of drug resistant bacteria. The rise of multidrug resistant TB (MDR-TB), i.e. which is resistant to at least isoniazid (INH) and rifampicin (RIF) requires the use of second-line drugs that are difficult to procure and are either less effective or more toxic with serious side-effects.[9-10] Resistance to MDR-TB was followed by emergence of extensively-drug resistant (XDR) and totally drug resistant strains of Mycobacterium tuberculosis.[11] Therefore, the detection and treatment of drug susceptible or single drug resistant TB is an important strategy for preventing the emergence of MDR and XDR-TB. Hence, it is quite essential to develop new strategies for the safe and cost-effective new antitubercular agents.

Molecular hybridization of potential pharmacophore scaffold has been an area of interest towards the design of new prototypes.[12-14] These molecules effectually address resistance problem and have an improved efficacy. Bearing in mind the hybrid concept along with the antitubercular potential of different moieties such as rifampin, ethambutol and isoniazid, it was planned to synthesize hybrid compounds comprising isoniazid moiety clubbed with other organic components and evaluate its anti-mycobacterial activity. Schiff bases of isoniazid have been reported for their potent antitubercular activity.[15-17] The reports suggest that the substitution at amine position as well as preparation of isoniazid derived Schiff bases may enhance antitubercular activity. Herein, we have synthesized two such isoniazid scaffolds by covalent addition on an aldehyde/diketone support (Fig.1a and 1b). The diketone derivative which contains two active isoniazid subunits and aldehyde conjugate with single isoniazid unit were evaluated for antitubercular activity. However, the clinical application of these compounds has been greatly limited due to its poor water solubility (practically insoluble in water) and stability, which severely reduces its bioavailability.[18,19]

[a.] *Department of Applied Chemistry, Cochin University of Science and Technology, Kochi-682 022, Kerala, India.*
[b.] *Department of Bacteriology, National Institute of Research in Tuberculosis, Chennai-600 031, Tamil Nadu, India.*
[c.] *Department of Chemistry, School of Physical Sciences, Central University of Kerala, Tejaswini Hills, Periye, Kasaragod-671 316, Kerala, India.*

Electronic Supplementary Information (ESI) available: [details of any supplementary information available should be included here]. See DOI: 10.1039/x0xx00000x

View Article Online
DOI: 10.1039/C9NJ06351J

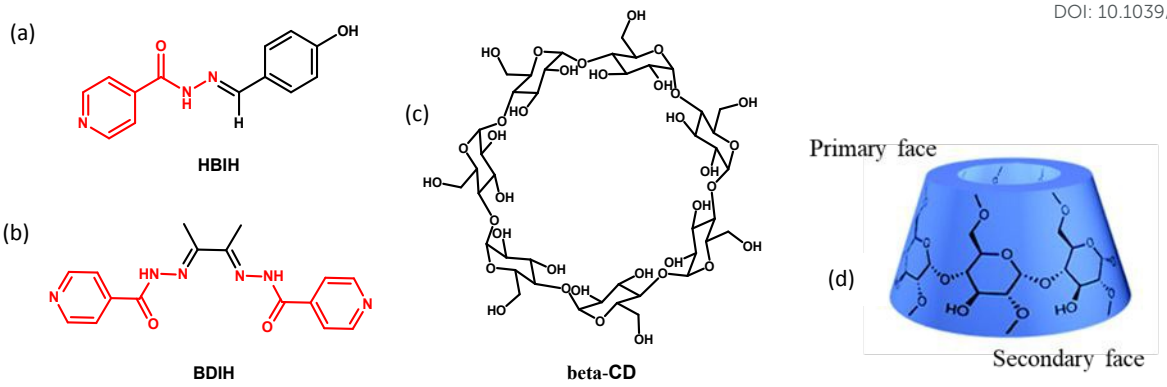

Fig. 1. 2D structure of the compounds under study (a) *p*-hydroxybenzaldehydeisonicotinylhydrazone (HBIH) (b) 2, 3-butanedione bisisonicotinylhydrazone (BDIH) (c) β-cyclodextrin (d) the trungated cone shape of β-cyclodextrin.

Design and synthesis of potent drug delivery systems are of immense importance for pharmaceutical applications. Smart, biodegradable, biocompatible targeting drug carriers have been developed in last few decades for the efficient transport of drug molecules through innovations in material chemistry. Various drug carriers like nanostructures, including polymers, dendrimers, silica or carbon based nanoparticles have been investigated as drug delivery systems.[20,21,22] Cyclodextrin (CD) complexation has been established as an effective method for the improvement of solubility and bioavailability of the many hydrophobic drug molecules.[23-26] CDs are cyclic oligosaccharides which consist of *α*-1,4-glycoside linkages. There are three recognized members of cyclodextrin, *α-, β-* and *γ*-CD, which are composed of six, seven and eight D-glucose units, respectively. The 1° and 2° hydroxyl groups present at the outer surface of CDs make the exterior hydrophilic, while the inner surface of CDs remain hydrophobic. The truncated cone-shape of CDs enables them to enclose the hydrophobic molecules to form inclusion complexes through non-covalent interaction without any complex chemical reactions.[27] The guest molecules can completely or partially enter the lipophilic cavity of CDs, therefore, CDs and its derivatives can improve the solubility of poorly soluble chemical entities. Among the three recognized members, *β*-Cyclodextrin (*β*-CD) is the most commonly used host molecule in pharmaceutical formulations due to their favorable cavity size, non-toxicity, biodegradability and economic price (Fig. 1c).[28,29]

So far, no research has been conducted on inclusion complexes comprising *β*-cyclodextrin and isoniazid Schiff bases. The aim of the present study was to utilize the complexation method to enhance the aqueous solubility and stability of the synthesized antitubercular isoniazid scaffolds. The inclusion complexes were prepared by co-precipitation and kneading method.[30] To explore host-guest interaction, the complexes were characterized via ^{1}H NMR, FT-IR, PXRD, SEM and phase-solubility studies. The results indicated that the water solubility of the compounds was significantly increased through *β*-CD complexation. The most probable structure of the inclusion complexes were proposed by molecular docking study. Finally, *in-vitro* anti-mycobacterial studies of inclusion complexes were performed to investigate whether the inhibitory effect retained after *β*-CD complexation.

2. Materials and Methods

Reagents and solvents were commercially purchased and used without further purification. FT-IR spectra were recorded in KBr by a JASCO FTIR 5300 spectrometer in the 400-4000 cm^{-1} range based on KBr disk technique. Electronic spectra were taken on a Spectro UV-vis Double beam UVD-3500 spectrometer in the 200-900 nm range. Powder X-ray diffraction (PXRD) measurements were carried out on a Bruker D8 Advance diffractometer equipped with graphite monochromatized Cu-Kα radiation (λ = 1.5405 Å). The morphology of the inclusion complexes was determined by scanning electron microscopy using JEOL Model JSM-6390LV. NMR spectra were recorded in DMSO-d6 using BRUKER AVIII (^{1}H NMR 500 MHz) spectrophotometer. Chemical shifts (δ) as given in terms of parts per million (ppm) are referenced to the residual solvent DMSO, ^{1}H NMR – 2.50 ppm.

2.1. Phase-solubility studies

Phase-solubility studies were performed according to the method reported by Higuchi and Connors.[31] Excess amount of HBIH/BDIH (20 mg) was added to 10 mL *β*-CD aqueous solution with increasing concentrations from 1 X 10^{-3} to 5 X 10^{-3} M respectively. The suspensions were sealed and stirred using magnetic stirrer at 200 rpm at room temperature for 48 hours until it reached equilibrium. The samples were then filtered through a 0.2 µm syringe filter. All samples were prepared in triplicate. The concentration of HBIH/BDIH in the filtrate was determined by a Spectro UV-vis Double beam UVD-3500 spectrometer in the 200-900 nm range. The phase-solubility profiles were obtained by plotting the solubility of HBIH/BDIH *vs*. the concentration of *β*-CD. The apparent stability constants (Ks) were calculated from phase-solubility diagrams according to the following equation:

$$\mathbf{Ks} = \frac{\mathbf{Slope}}{\mathbf{S_0(1 - Slope)}}$$

where S_0 is the solubility of HBIH/BDIH at 25 °C in the absence of *β*-CD and slope means the corresponding slope of the phase-solubility diagrams.

2.2. Molecular Modelling and docking studies

The most probable structure of *β*-CD/HBIH and *β*-CD/BDIH inclusion complexes were determined by molecular docking studies using Autodock Tools 1.5.6.[32] The three-dimensional structure of *β*-cyclodextrin was extracted from the PDB file 3CGT, which was downloaded from the RCSB Protein Data Bank. The 2D structure of isoniazid-hybrid molecules were drawn using ChemDraw and converted into a 3D structure using Avagadro 1.0.1 software.[33] The ligand was prepared for docking by defining rotatable bonds. The Autodock program was run by setting *β*-CD as a rigid receptor and guest molecule as the flexible ligand. The search grid of the *β*-cyclodextrin was identified as center_x: 58.435, center_y: 11.947, and center_z: 8.888, with dimensions of size_x: 40, size_y: 40, and size_z: 40. The rest use default parameters. The program gave numerous feasible docked models for the most plausible structure based on the energetic parameters of the *β*-CD inclusion complex.

High-resolution crystallographic structures of enzymes (cocrystallized with either inhibitors or the natural substrates) were downloaded from www.rcsb.org. The three-dimensional structure of 4FDN and 1W2G was downloaded from the Protein Data Bank. The co-crystallized ligands were first stripped from the bound enzymes and polar hydrogen atoms were added with the aid of Discovery studio.[34] Autodock 4.1 was used to dock protein and ligands. The Lamarckian Genetic Algorithm from MGLTools (http://mgltools.scripps.edu/) was used to search energetically supported binding modes.[35] Each docking experiment was derived from 10 different runs that were set to terminate after a maximum of 250000 energy evaluations. The population size was set to 150. AutoDockTools 1.5.6 were implemented to build the Autogrid box between the protein and ligands. The grid center was chosen on the protein residues and the dimensions were 100×100×100 autogrid points (x,y,z directions) with 0.26 Å spacing. All rotatable torsion was released during docking in order that the confomation of inhibitor become flexible. The best-scoring pose as judged by the binding energy of the ligand-receptor complex was visually analyzed using Discovery Studio 2017R2 and Chimera 1.13.1 softwares.[36]

2.3. *In-vitro* anti-tubercular activity

LRP Assay: Luciferase Reporter Phage Assay was carried out to determine the anti-tubercular activity of the test compounds.[37,38] Bacterial cell suspension was prepared by inoculating the log phase culture of *Mycobacterium tuberculosis* H37Rv strain at 37 °C in Middlebrook 7H9 media supplemented with 5% glycerol and 10% albumin dextrose complex. Assay was done using different concentration of test compounds and DMSO 1% was used as the solvent control. About 350 μL of G7H9 broth was taken in cryovials and added 50 μL of test compound followed by 100 μL of *M. tuberculosis* cell suspension. All the vials were incubated at 37 °C for 72 hours. After incubation, 50 μL of high titre mycobacteriophage phAE129 and 40 μL of 0.1M $CaCl_2$ solutions were added to the test and control vials and further incubated at 37 °C for 4 hours. After incubation, 100 μL and 500 μL from each vial was transferred to luminometer cuvette. About 100 μL of D-luciferin was added and relative light unit (RLU) was measured in luminometer. RLU reduction by 50% or more when compared to control was considered as having anti-tubercular activity.

$$\% \text{ RLU reduction} = \frac{\text{Control RLU} - \text{Test RLU}}{\text{Control RLU}} \times 100$$

MIC by Cord formation Assay: The assay is based on the characteristic cord-like formation of Mtb in liquid culture media when imaged under an inverted light microscope. Cord factor (trehalose 6,6′ dimycolate), a glycolipid that is present on Mtb cell wall promotes adhesion of bacterial cells and results in the formation of serpentine cords. In the presence of anti-TB drugs, drug susceptible Mtb strains do not form cord-like structures, whereas cord formation is unaffected with DR-Mtb strains.

Minimum Inhibitory Concentrations (MIC) of the inclusion complexes were tested at the concentration ranging from 10 to 500 µg/ml against the MDR clinical isolates and H37Rv. Culture suspensions were prepared by growing the inoculum in Middlebrook 7H9 broth. To prepare the suspension for inoculation, the cultures were vortexed, left for 30 sec to allow the setting of heavy particles. The culture suspension was adjusted to reach a turbidity that matched the optical density of a 1 MacFarland standard and diluted at 1:10 ratio so that each well contains $1x10^5$ cells. Rifampicin at critical concentration of 1µg/mL was kept as drug control. Culture control and solvent control (DMSO) were included in the assay. The plates were incubated at 37 °C for 5 days. After 5 days, the plates were observed under microscope for determining gradation based on the serpentine cord formation of Mtb culture growth. All the tests were performed in triplicates in a microtiter plate and the concentration of compounds which completely inhibit the growth of the Mtb cultures were considered as MIC.[39]

2.4. *In-vitro* cell viability studies

Cell viability studies were carried out against the mammalian mouse fibroblast cell lines L929, obtained from National Centre for Cell Science (NCCS), Pune, India). In a 96-well plate, 100 µl cell suspension ($5x10^3$ cells/well) was seeded and incubated at 37 ºC in a humidified 5% CO_2 incubator. Compound stock solutions were prepared by dissolving 1 mg of sample in 1 mL DMEM (Dulbecco's modified Eagles medium). After 24 hours the growth medium was removed, freshly prepared each complexes in 500 µL of 5% DMEM were five times serially diluted by two fold dilution (100, 50, 25, 12.5, 6.25 µg) and each concentration of 100 µL were added in triplicates to the respective wells and incubated at 37 ºC. Non treated control cells were also maintained. Entire plate was observed after 24 hours of treatment in an inverted phase contrast tissue culture microscope. After the treatment, the solutions were flicked off from the wells and 30 µL of reconstituted MTT (3-(4,5-dimethylthiazol-2-yl)-2,5-diphenyltetrazolium bromide) solution was added to all test and cell control wells and then incubated for 4 hours. 100 µL of MTT solubilization solution (DMSO) was then added and the wells were mixed gently by pipetting up and down in order to solubilize the formazan crystals. The absorbance values were measured by using microplate reader at a wavelength of 540 nm.[40]

$$\text{Percentage of viability} = \frac{\text{Mean OD Samples}}{\text{Mean OD of control group}} \text{ X } 100$$

View Article Online
DOI: 10.1039/C9NJ06351J

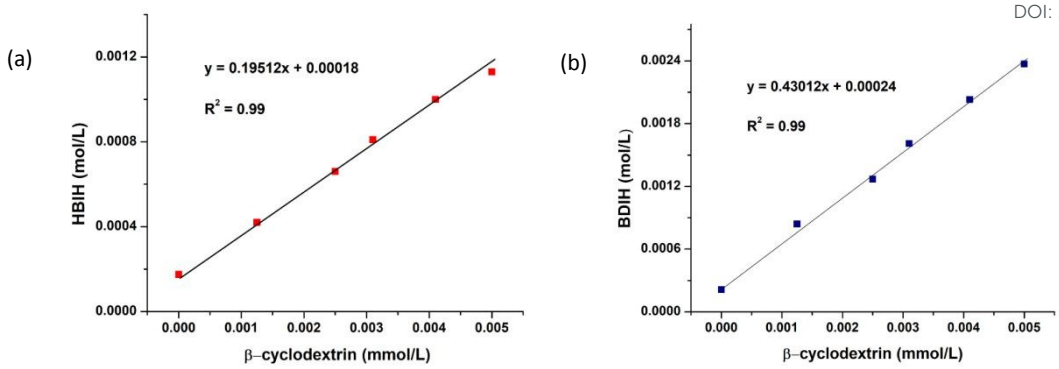

Fig. 2. Phase-solubility diagrams of HBIH (a) and BDIH (b) with *β*-CD at 25 °C.

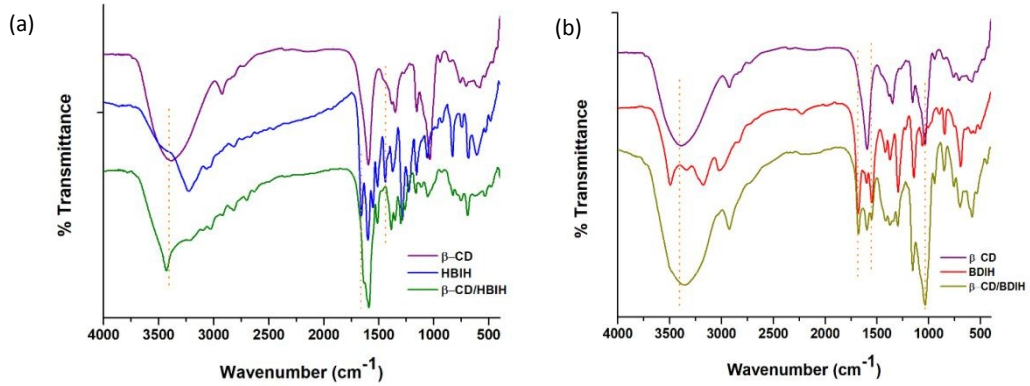

Fig. 3. FTIR results (a) spectra of HBIH, *β*-CD and *β*-CD/HBIH inclusion complex (b) spectra of BDIH, *β*-CD and *β*-CD/BDIH inclusion complex.

The LC50 value was calculated by concentration-response graph fitting using ED50 PLUS V1.0 Software.

2.5. Synthesis of *p*-hydroxybenzaldehydeisonicotinyl hydrazone (HBIH) and 2, 3-butanedione isonicotinylhydrazone (BDIH)

The synthesis of HBIH and BDIH involved condensation of isoniazid and selected aldehyde/diketone in methanol with continuous stirring at 60 °C for 2 hours. The clear solutions were then transferred to beakers for slow evaporation at room temperature. The isolated crystalline product was subjected to characterization by spectroscopic (NMR, IR and UV) and X-ray diffraction methods.

2.6. Preparation of *β*-cyclodextrin inclusion complexes

The solid inclusion complexes were prepared by co-precipitation and kneading method.

2.6.1. Synthesis of *β*-CD/HBIH

The inclusion complex *β*-CD/HBIH was prepared in a 1:1 ratio *via* the co-precipitation method.[41] 1.135 g (1 mmol) of *β*-CD was dissolved in 20 mL of de-ionized hot water. Subsequently, 0.241 g (1 mmol) of HBIH dissolved in 20 mL hot ethanol was added slowly to the aqueous *β*-CD solution. The solution was stirred for 2 h at room temperature. The precipitated complex was recovered by filtration and washed with a small amount of ethanol and water to remove unreacted HBIH and *β*-CD. The product was dried, collected, and stored in airtight containers for further use.

2.6.2. Synthesis of *β*-CD/BDIH

1.135 g (1 mmol) of *β*-CD and 0.324 g (1 mmol) of BDIH were weighed and dry triturated in a mortar for 15 min. The mixture was then kneaded with 3:1 ethanol/water mixture for about 30 min. During this process, an appropriate quantity of the solvent was added in order to maintain a suitable consistency required for kneading. The product was dried at 50 °C and stored.

2.6.3. Preparation of physical mixture

The physical mixtures was prepared by simply mixing HBIH/BDIH with *β*-CD in the same molar ratio as the inclusion complex. The mixture was ground with a mortar for 15 min to ensure uniform mixing.

3. Result and Discussion

3.1. Characterization of *β*-cyclodextrin inclusion complexes

3.1.1. Phase-solubility studies

The phase-solubility studies were carried for the evaluation of inclusion effect, stoichiometric ratio and the determination of the stability constant (K_s). The solubility of *β*-CD in water has been determined to be 1.8 g/100 mL and for HBIH and BDIH it is found to be 1.6 mg/100 mL and 1.9 mg/100 mL respectively. As shown in Figs. 2a and b, the aqueous solubility of HBIH and BDIH was positively correlated with the increase of *β*-CD

concentration. Based on Higuchi and Connors's theory, these two linear host–guest correlations can be classified as A_L type since the slope values are less than 1 (0.2107 and 0.4403 for HBIH and BDIH respectively). This suggests a 1:1 stoichiometry for the two complexes. The apparent stability constants (K_s) were calculated from the straight line of phase solubility diagrams as per the stability constant equation (K_s). The value of K_s is most often between 50 and 2000 M^{-1}. The K_s value for *β*-CD/HBIH was equal to 1329 M^{-1}, and that of *β*-CD/BDIH was equal to 3728 M^{-1}. The higher values indicated a strong tendency of the guest molecules to entrap into the interior of *β*-CD.[42] Moreover, if the stability constant is too weak, there will be only little improvement in solubility of HBIH/BDIH.[43] The findings revealed that the solubility of the compounds was significantly increased in presence of CDs, which indicated a great solubilizing potential for HBIH/BDIH by β-CD.

3.1.2. FTIR analysis

The infrared band usually shifts or the intensity changes after the guest molecule is encapsulated by *β*-cyclodextrin due to the loss of bending and vibrating peaks of guest molecules. Fig. 3 shows the FTIR spectra of HBIH, BDIH *β*-CD, *β*-CD/HBIH and *β*-CD/BDIH in the region of 4000-500 cm^{-1}. The spectrum of *β*-cyclodextrin is characterized by a broad band with a transmittance peak of 3396 cm^{-1} (for the –OH stretching vibration), 2920 cm^{-1} (for the C–H stretching vibration), 1036 cm^{-1} (for the symmetric C–O–C stretching vibration). The characteristic functional groups of HBIH and BDIH (Figs. 3a and b) are located at 1658 and 1684 cm^{-1} (for the C=N stretching vibration), 1600 and 1598 cm^{-1} (for the C=O stretching vibration), 3452 and 3489 cm^{-1} (for the N–H stretching vibration) respectively.[44,45] The spectra of the two inclusion complexes (*β*-CD/HBIH and *β*-CD/BDIH) are comparable to *β*-CD. It is apparent that no additional peaks are recognized in the inclusion complexes, which mean no chemical reaction occurred between the guest molecules and CD. However, spectra exhibit some modifications in the vibrational modes of guest molecules and *β*-CD. The C=O/C=N stretching vibrations of guest molecules are absent/weakened in the complex, establishing the diminished interaction among the inclusion complex molecules. Moreover, the free hydroxyl stretching frequency of *β*-CD is found to be narrowed (*β*-CD/HBIH)/shifted to lower region (*β*-CD/BDIH) due to the involvement of hydrogen bonding and other secondary interactions with the guest molecule, which also supports the encapsulation of the guest molecules into the cavity of *β*-CD.

3.1.3. Powder X-ray Diffraction

Further evidence for the formation of the *β*-CD inclusion complex was obtained from XRD, which has been proven to be an effective method for investigating CDs and their inclusion complexes in the powder or microcrystalline state. As indicated in Fig. 4, the XRD patterns of HBIH, BDIH and *β*-CD exhibited prominent signatures characteristic of its crystallinity. The diffractogram of the 1:1 physical mixture was basically the superposition of the signal profiles of *β*-CD and HBIH/BDIH, indicating that no chemical association has occurred and both kept their original physical characteristics. By contrast, the diffraction profile of inclusion complexes showed a sharply distinct pattern from that of the physical mixture indicating a new crystalline phase and suggesting inclusion behavior between guest molecule and *β*-CD. However, the characteristic peaks of guest molecule (HBIH/BDIH) have disappeared from the diffraction pattern of the inclusion complex. New peaks display a few crystalline peaks for guest molecules with decreased intensities, indicating that new complexes were formed. Although the diffraction peaks were obviously weakened, the main diffraction peaks were similar to *β*-CD. The above results also could be verified by SEM.

3.1.4. SEM

SEM studies were conducted to investigate the morphology of *β*-CD, HBIH, BDIH and their inclusion complexes (Fig. 5). Pure HBIH existed in block shaped crystals with medium dimensions, whereas, BDIH was characterized by flowerlike morphology. *β*-CD appeared as irregular crystals with unclear edges (Fig. 5a). But, it was found that, the morphology and size of particles in the inclusion complexes were entirely different from the constituents. *β*-CD/HBIH has a plate-like structure and was quite different from *β*-CD and HBIHs, which confirms the formation of inclusion complex.[46] In similar test, *β*-CD/BDIH and BDIH appeared to be different in sizes and shapes. The morphological change of BDIH from flower-like structure to smaller aggregates is due to the encapsulation in the cavities of *β*-CD. The images of physical mixtures revealed that, they were similar to the simple superposition of both constituents and HBIH/BDIH particles were found to be adhered on the surface of *β*-CD particles (Figs. 5d and g).

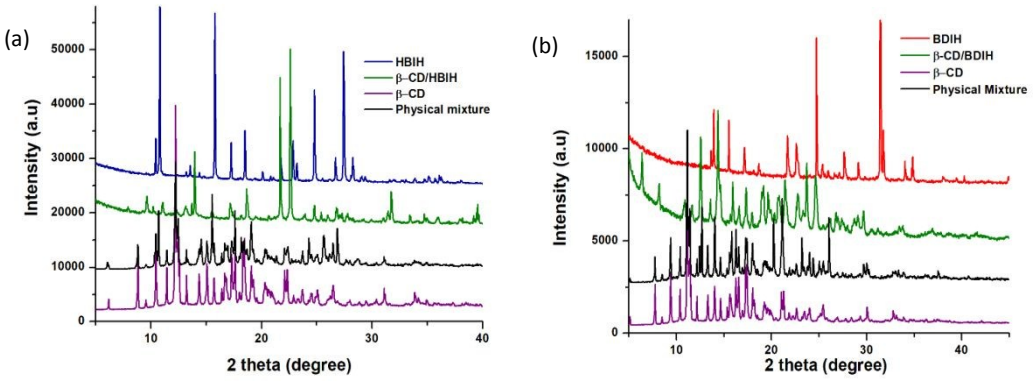

Fig. 4. Results of PXRD (a) HBIH, *β*-CD, Inclusion complex of *β*-CD/HBIH and physical mixtrue of *β*-CD and HBIH (b) BDIH, *β*-CD, Inclusion complex of *β*-CD/BDIH and physical mixtrue of *β*-CD and BDIH.

View Article Online
DOI: 10.1039/C9NJ06351J

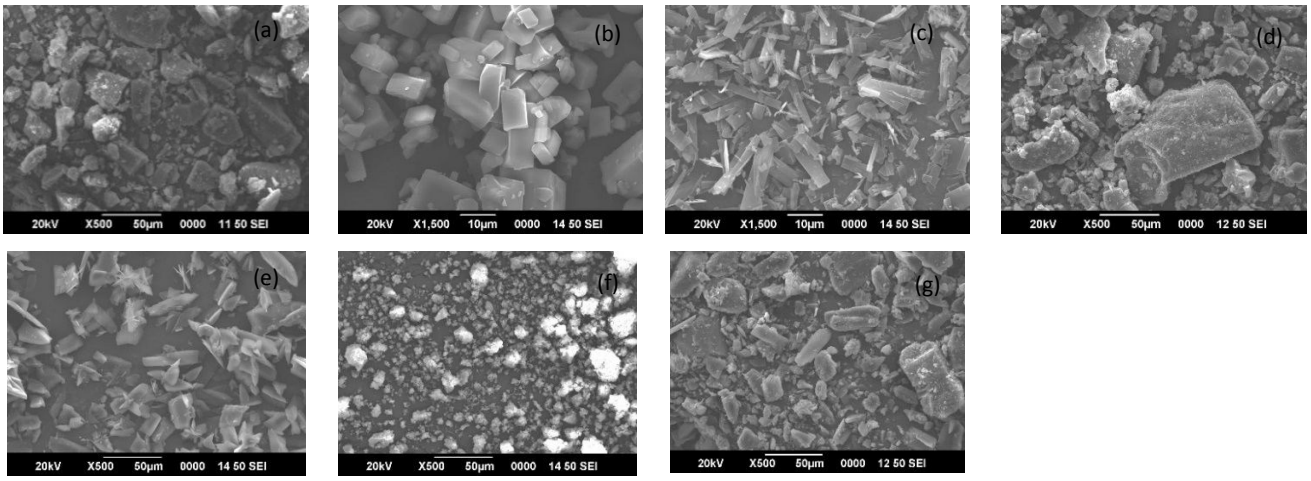

Fig. 5. Scanning electron microscopy image of (a) *β*-CD (b) HBIH (c) *β*-CD/HBIH inclusion complex (d) Physical mixture of *β*-CD and HBIH (e) BDIH (f) *β*-CD/BDIH inclusion complex (g) Physical mixture of *β*-CD and BDIH.

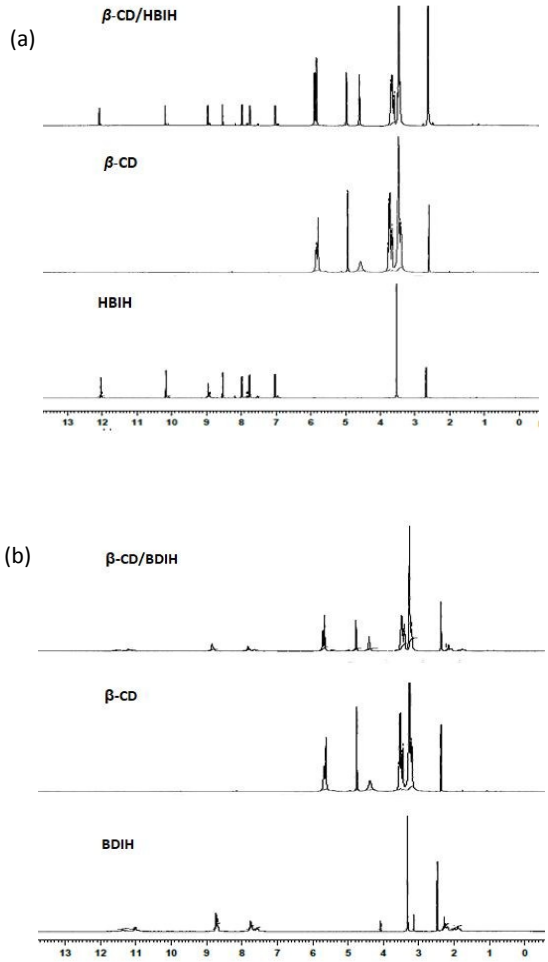

Fig. 6. ^{1}H NMR spectra in DMSO (a) HBIH, *β*-CD, *β*-CD/HBIH (b) BDIH, *β*-CD, *β*-CD/BDIH complex.

3.1.5. NMR experiments

NMR gave the most powerful evidences to support the formation of inclusion complexes. The chemical shift of inclusion complexes were affected during complexation and the changes were used to explain the host–guest interaction between β-CD and guest molecules.47 Since the host and guest molecules do not form any chemical bonds, the interaction mainly relies on intermolecular forces existing between molecules. We measured the 1H-NMR spectra of the HBIH, BDIH, β-CD and their inclusion complexes in DMSO. The spectra of the inclusion complexes showed all of the expected proton signals of guest molecules and cyclodextrin, in agreement with the formation of the inclusion complex (Fig 6a and b).

When the inclusion complex is formed, the chemical shift values of H-3 and H-5 protons showed significant changes and migrated to the high field due to magnetic anisotropy effects of guest molecule. The result might be due to H-3 and H-5 in β-cyclodextrin molecule was located inside the cyclodextrin cavity. Whereas, the chemical shift values of H-2, H-4 and H-6 protons outside the cavity were least affected and changed a little after cyclodextrin complexation. In order to further explore the inclusion mode, the chemical shift variations of guest molecules in comparison with inclusion form were also examined. The most significant changes were observed for NH protons of both HBIH and BDIH and OH proton of HBIH. Thus, it was reasonable to deduce that they are actively involved in hydrogen bonding with β-CD. The chemical shift changes in free and complexed forms of cyclodextrin and guest molecules are listed in Table S1.

3.2. Molecular Modelling

To further scrutinize the binding affinity and key interactions between the guest molecules HBIH/BDIH and β-cyclodextrin receptor, docking studies were performed using AutoDock Tools.3228. The ligands were docked into the binding pocket of the

View Article Online
DOI: 10.1039/C9NJ06351J

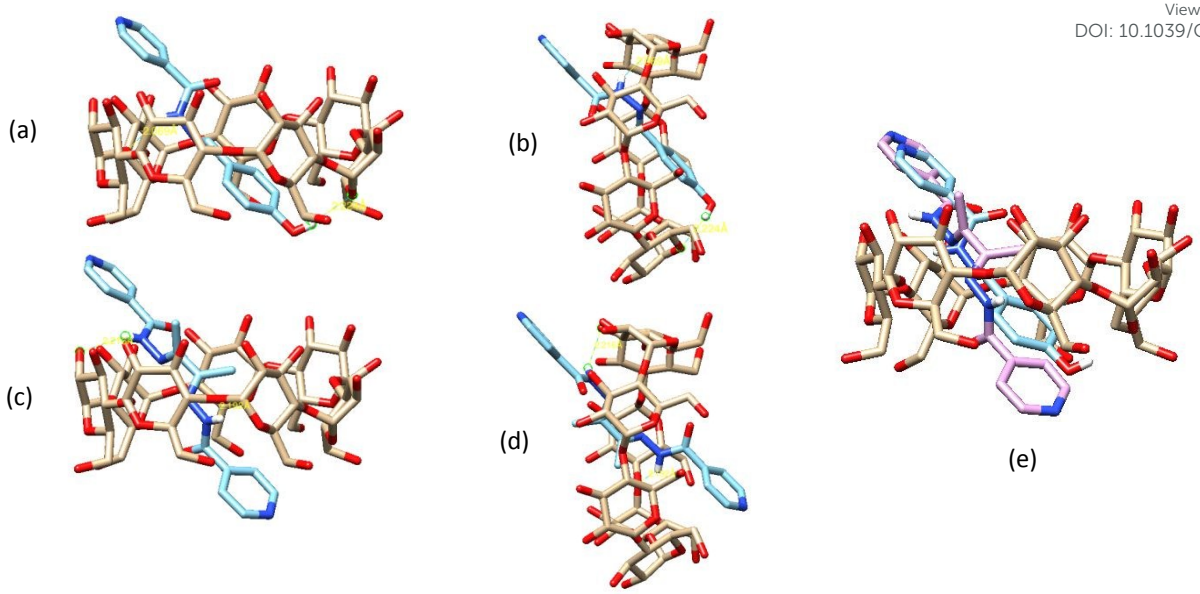

Fig. 7. The docking modelling studies: 3D structures of *β*-CD/HBIH inclusion complex, front view (a) and side view (b) 3D structures of *β*-CD/BDIH inclusion complex, front view) (c) and side view (d) overlay structure (e).

β-cyclodextrin and the most probable conformation obtained are shown in Fig. 7. Results showed that HBIH and BDIH were effectively combined with β-CD in 1:1 ratio. The inclusion complexes generated by the docking algorithm in each case were clustered based on binding energy and root mean square deviation (RMSD) of their conformation. For HBIH, the estimated free energy of binding for the best pose was -5.33 kcal/mol, while BDIH showed binding energy of -6.02 kcal/mol. Molecular modeling results revealed that the guest molecules snugly fit into the hydrophobic host cavity with a twisted linear conformation (change from *trans* to *cis* configuration). Detailed analysis revealed two key hydrogen bonding interactions with distances of 2.06 and 2.22 Å for *β*-CD/HBIH and 2.19 and 2.21 Å for *β*-CD/BDIH (Figs. 7a and c) are present in the complexes. These interactions aided guest molecules to anchor to the binding site of β-cyclodextrin. The pyridine ring of HBIH lies in a more elevated position towards the secondary rim of *β*-CD which allows a better interaction with hydroxyl group and primary rim of *β*-CD. While, *β*-CD/BDIH cluster with highest affinity conformation have a symmetrical orientation towards the wider and narrower end of the cyclodextrin cavity. Fig. 7e presents an overlay of the binding mode of guest molecules over *β*-CD.

3.3. Pharmacology

Preliminay anti-TB screening was performed on compounds HBIH and BDIH at concentrations 100 and 500 µg/mL against the drug sensitive strain of *Mycobacterium tuberculosis H37Rv* (ATCC-27294) using the LRP (Luciferase Reporter Mycobacteriophage) assay, as reported by Jacobs *et al.*[37] Since isoniazid was used as the basis for the development of structural analogues, the compounds showed good activity with more than 80% inhibition (Table S2). However, HBIH and BDIH have a major inconvenience. Being hydrophobic it cannot be dissolved and unavailable for adsorption in the gastrointestinal tract, which severely reduces its bioavailability. Considering the clinical application and stability of these compounds, we have carried out further *in-vitro* studies on encapsulated complexes, i.e. *β*-CD/HBIH and *β*-CD/BDIH inclusion complexes.

The inclusion complexes were assayed for determination of MIC against different Mtb clinical isolates, drug sensitive and resistant strains. MIC is the concentration required to completely inhibit (more than 98%) the Mtb growth. Table 1 shows the minimal inhibitory concentration (MIC) of the inclusion complexes against H37Rv strain and MDR strains. Due to crystal formation, we couldn't record the MIC of *β*-CD/BDIH against H37Rv strain. Compared to other clinically active drugs, percent entrapment of drug will be small in encapsulated complexes.[30] On this account, we have used encapsulated isoniazid drug molecule as a standard for both drug sensitive and resistant strains (high-dose isoniazid is recommended by WHO for MDR-TB) for finer comparison of MIC.[43,48] The MIC of standard rifampicin and isoniazid was also given in Table 1.

The MIC value of *β*-CD/HBIH (50 µg/mL) was found to be better as compared to diketone analogue *β*-CD/BDIH against the drug resistant strains. Gratifyingly, the results showed that the complex *β*-CD/HBIH exhibit biological activity greater than the first line drug isoniazid inclusion complex, and clearly could be considered a good starting point for further studies. The complex also showed good activity against drug sensitive Mtb strains; whereas the standard exhibited moderate activity against resistant strains with MIC value of >100 µg/mL (Table 1). As both HBIH and BDIH inclusion complexes have activity against resistant strain, these molecules can serve as lead for further generation of more active compounds. The complexes were further subjected to cell viability studies.

View Article Online
DOI: 10.1039/C9NJ06351J

Table 1. MIC (Minimum Inhibitory Concentration) of *β*-CD/HBIH and *β*-CD/BDIH against H37Rv and MDR strains

Compound Name	Concentration (µg/ml)							
	500	400	300	200	100	50	10	MIC
Mycobacterium tuberculosis H37Rv								
β-CD/BDIH	CRF	CRF	CRF	CRF	CRF	CRF	Sc	--
β-CD/HBIH	N	N	N	N	N	N	Sc	50
β-CD/IH	N	N	N	N	N	Sc	Sc	100
Mycobacterium tuberculosis MDR Strain								
β-CD/BDIH	N	N	N	Sc	Sc	CRF	Sc	300
β-CD/HBIH	N	N	N	N	N	N	Sc	50
β-CD/IH	N	N	N	Sc	Sc	Sc	Sc	300
IH (Isoniazid)	--	--	--	--	--	--	--	0.02
Rif (Rifampicin)	--	--	--	--	--	--	--	0.1

CRF- Crystal formation, N-negative growth, Sc-scanty growth, IH-isoniazid

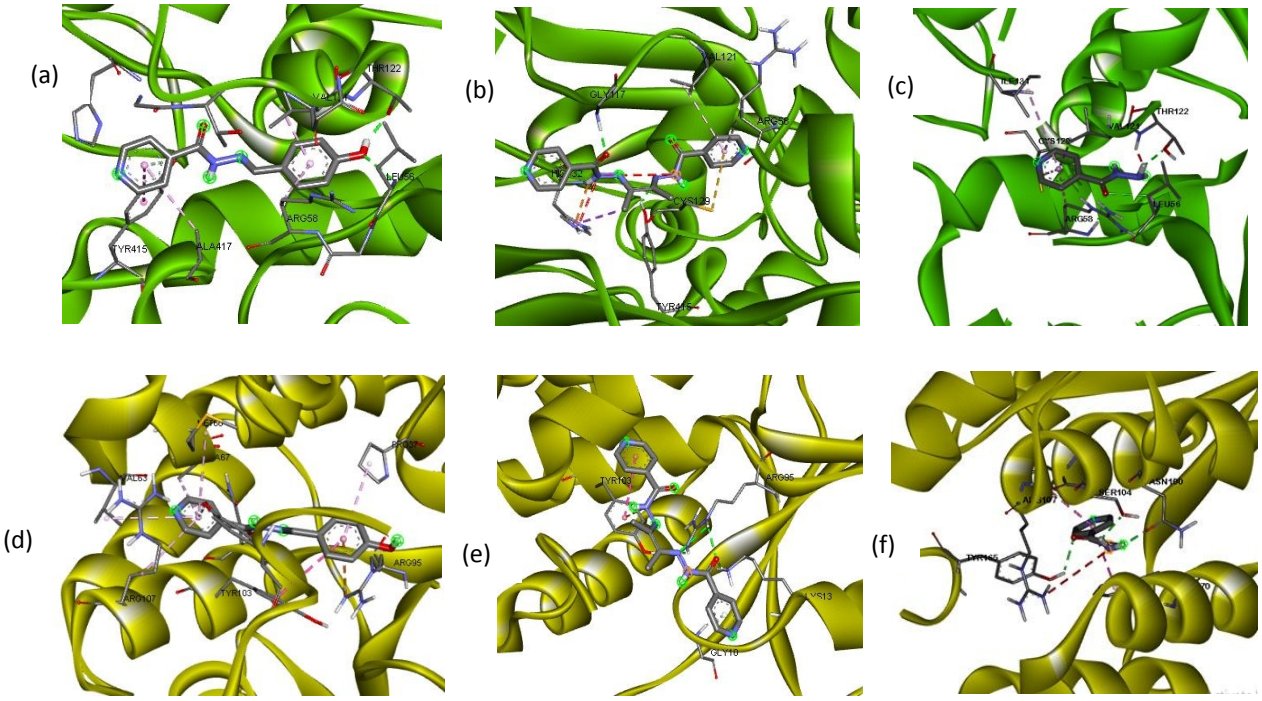

Fig. 8. 3D view of the binding of HBIH (a), BDIH (b) and IH (c) with the active site of protein DprE1. Binding of HBIH (d), BDIH (e) and IH (f) with Thymidine Monophosphate Kinase.

3.4. Docking study

In silico based approaches have provided a new perspective in the growth of highly efficient chemical leads for the development of new chemical formulations against TB.[49-51] With the aim of rationalizing the promising antitubercular activity obtained for isoniazid-hybrid compounds, molecular docking study was performed to support the mode of action, interaction and preferred binding sites of the targeted compounds with the active sites of the bacterial protein.

Many well-known anti-TB drugs are known to target the biosynthetic pathways that involve the production of macromolecules such as proteins, nucleic acids, or cell wall polymers.[52] In this regard, decaprenylphosphoryl-*β*-D-ribose-2'-epimerase (DprE1) was chosen as the bacterial protein-bearing active site. DprE1 is a key precursor for the synthesis of cell wall, and it is a highly vulnerable, fully validated tuberculosis drug target.[53] For the development of new drugs, targets should be specific to *Mycobacteria* to control the transfer of resistance factors from other bacteria. In this respect, inhibition of nucleotide biosynthesis

pathway can be an important target in antitubercular drug discovery particularly for the treatment of MDR TB. Thymidine monophosphate kinase (TMPKinase) has been suggested as a high-confidence MDR drug target to develop new anti-tubercular agents, which is a key enzyme involved in nucleotide metabolism.[54] Subsequently, we have performed docking studies against DprE1 and Thymidine monophosphate kinase to find out the best possible mode of action and molecular basis of interaction with the synthesized hybrids of isoniazid. This study provided valuable guidance for rationally designing more potent inhibitors for treatment of TB.

From the ensuing docked structures, it is clear that the ligand molecules could easily fit into the active site of DprE1 and thymidine monophosphate kinase with very similar orientations and occupying positions very close to that of the native ligand in the crystal structure. Table S3 shows the interaction energies that occur when ligands bind to the protein of the targeted compounds. The lowest energy docked conformation of the targeted candidates is considered as efficient binding, which signifies the energy required for a ligand to cover the entire surface of the enzyme. Lower the value of binding energy, stronger is the affinity towards the active site. Both the compounds showed better receptor interaction with superior docking score values over the range of -6.63 to -7.99, compared to the standard drug isoniazid with docking scores of -5.18 and -5.10, respectively against DprE1 and TMPKinase (Fig 8c and f).

All the ligand-receptor complexes were stabilized by non-bonded secondary interactions through the active site residues and all interactions were observed to be conserved with reference to the standard inhibitors. The hydrazone linkage reduced torsional stress and increased the ability of the compounds to rotate and situate flawlessly within the active site. Binding mode analysis suggested that the diketone derivative with two isoniazid moieties displayed significant interaction with active residues. Amino nitrogen and carbonyl oxygen, which act as strong hydrogen bond donor and acceptor respectively, allowed more interaction to take place and therefore showed higher docking scores. Besides being stabilized by strong hydrogen bonding interaction with HIS 132, TYR 415 and GLY 117, BDIH-DprE1 complex formed strong pi-alkyl interactions with VAL 121 and ARG 58 (Figs. 8b and Fig. S1). Likewise, HBIH-DprE1 complex also showed two types of forces stabilizing interaction with the binding site residues (Fig. 8a). A strong directional interaction with hydroxyl group of HBIH and the backbone oxygen of THR 122 and amine nitrogen of LEU 56 and π-alkyl interactions quite similar to BDIH-DprE1 complex. Comparison between activity for compound HBIH and BDIH with TMPKinase showed that hydrogen bonding interactions were significantly decreased for HBIH-TMPKinase complex (Fig. 8d and e). However, the complex was stabilized by a group of π-alkyl interactions (Fig. S2). The enhanced binding affinity of BDIH can be attributed to the two prominent hydrogen bonding interaction with LYS 13 and ARG 95 residues of the protein. Analysis of other docking parameters revealed low inhibition constants (K_i) for all ligand-receptor complexes, which indicates potency of an inhibitor towards a protein. If K_i is smaller, less drug is needed to inhibit the enzyme activity. The vdW, hydrogen bond and dissolved energy value predicted the ligands were well attached to the active site of the target molecule.[55] Similarly, the electrostatic energy (change on the electrostatic non bounded energy of ligand or protein upon binding) is found to be negative in all cases (Table 2). Thus, a strong network of thermodynamic interactions observed between ligand-receptor complexes, which account for its good *in-silico* binding and provides a hint for its significant *in-vitro* antitubercular activity.

3.5. Cell viability studies

In-vitro cell viability studies are the first step to assess the toxicity of newly synthesized bioactive compounds. The morphologic changes to mammalian L929 fibroblasts cell lines after treatment with different concentration of inclusion complexes were analyzed by phase contrast microscopy and shown in Fig S3. They did not demonstrate any significant detrimental changes. The results of MTT assay are presented in Fig. 9. The viability of cell lines was assessed after 24 hours of incubation with complexes at different concentrations ranging from 6.25-100 µg/mL. The control cells which are not treated with any compound have shown 100% viability. Viability values of 73-96% were obtained for the complexes over the whole range of investigated concentrations. The values never dropped below 70% even at the highest concentration (100 µg/mL).[56] The LC50 values for the complexes studied were found to be >50 µg/mL (268.741 µg/mL and 203.425 µg/mL respectively for *β*-CD/HBIH and *β*-CD/BDIH) indicating that the complexes are non-toxic.

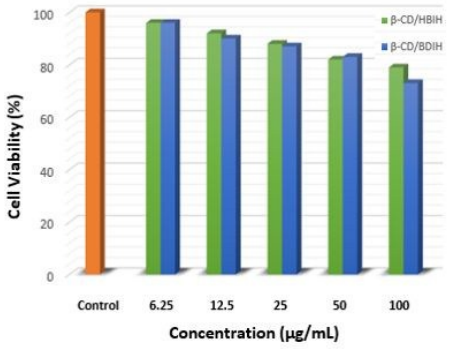

Fig. 9. Cell viability of control, inclusion complexes *β*-CD/HBIH and *β*-CD/BDIH on L929 cells at different concentrations (100, 50, 25, 12.5, and 6.25 µg/mL).

Conclusion

In the present study, we have demonstrated the feasibility of *β*-CD to encapsulate two isoniazid Schiff base compounds *via* inclusion complexation. The compounds were successfully encapsulated into the cavity of *β*-CD and the formation of the inclusion complex was confirmed by FTIR, PXRD, SEM, ^{1}H NMR and phase-solubility studies. To prove the experimental findings and predict the stable molecular structure of the inclusion complexes, molecular docking studies were performed and supramolecular interactions were analyzed. The water solubility of the poorly soluble compounds were significantly improved by complexation with *β*-CD in a 1:1 stoichiometry.

Furthermore, we studied the anti-mycobacterial activity and docking correlations of the synthesized complexes. The complexes were found to be active against Mtb and *β*-CD/HBIH showed better activity compared to isoniazid inclusion complex. These complexes open a new door in anti-TB drug design perspective by providing highly specific, non-toxic candidates. Given the easy preparation and environmentally friendly process for inclusion complexes, it is a promising way to design novel prototypes of isoniazid congeners with excellent water solubility and bioavailability for future pharmaceutical applications.

Conflicts of interest

"There are no conflicts to declare".

Acknowledgements

Lincy Tom gratefully acknowledges CSIR, New Delhi, India for financial support in the form of a Senior Research Fellowship. The authors are thankful to the Sophisticated Analytical Instrumentation Facility (SAIF), Kochi and IIT madras for SEM, PXRD and NMR studies. We thank National Institute for Research in Tuberculosis, Chennai for anti-TB studies. We also thank Biogenix Research center, Thiruvananthapuram for cell viability studies.

References

1. D.A Enarson and J. F Murray, Global Epidemiology of Tuberculosis. In Tuberculosis; Rom, (W. N., Garay, S., Eds.), Little Brown and Co.: Boston, 1996, pp 57–75.
2. World Health Organization, Global Tuberculosis Control, WHO Report, 2018.
3. H. Jnawali and S. Ryoo, First- and second-line drugs and drug resistance. Available at https://www.intechopen.com/books/tuberculosis-current-issues-in-diagnosis-and-management/ *First-and-second-line-drugs-and-drug-resistance*. 2013
4. M. Gengenbacher and S. Kaufmann, *FEMS Microbiol. Rev.,* 2012 **36**, 514–532.
5. H. Meyer and J. Mally, *Monatsh*, 1912, **33***,* 393-414.
6. S. P. Klemens, C.A. Sharpe and M. H. Cynamon, *Antimicrob. Agents and Chemother.*, 1996, **40** (1), 14–16.
7. M.E. Villarino, R. Ridzon, P.C. Weismuller, M. Elcock, R.M. Maxwell, J. Meador, P.J. Smith, M.L. Carson, L.J. Geiter, *Am. J. Respir. Crit. Care Med.*, 1997, **155**(5), 1735-1738.
8. H. C. Hinshaw, M. D., M. M. Pyle, W. H. Feldman and D. V. M. *Am. J. Med.,* 1947, **2**(5), 429–435.
9. A. J. J. Wood and M. D. Iseman, *N. Engl. J. Med.,* 1993, **329** (11), 784–791.
10. S. Ramaswamy and J.M. Musser, *Tuber. Lung Dis.*, 1998, **79**(1), 3–29.
11. A. Velayati, P. Farnia and M. Masjedi, *Int. J. Clin. Exp. Med.,* 2013, **6**(4), 307–309.
12. R. Saha, M. M. Alam and M. Akhter, *RSC Adv.,* 2015, **5**(17), 12807-12820.
13. R. Revathi, R. V.Perumal, K. S. R. Pai, G. Arunkumar, D. Sriram and S. G. Kini, *Drug Des., Devel. Ther.,* 2015*, **9***, 3779–3787.
14. M.M. Pisal, L. U. Nawale, M.D. Patil, S. G. Bhansali, J. M. Gajbhiye, D. Sarkar, S. P. Chavan and H. B. Borate, *Eur. J. Med. Chem.*, 2017, **127**, 459-469.
15. A. Kajal, S. Bala, S. Kamboj, N. Sharma and V. Saini, *J. Catal*, Article ID 893512, 2013, 1–14.
16. M. J. Hearn, M. H. Cynamon, M. F. Chen, R. Coppins, J. Davis, H. Joo-On Kang, A. Noble, B. Tu-Sekine, M. S. Terrot, D. Trombino, M.Thai, E.R. Webster and R. Wilson *Eur. J. Med. Chem.,* 2009, **4**(10), 4169–4178.
17. P. Dandawate, K. Vemuri, K. V. Swamy, E. M. Khan, M. Sritharan, and S. Padhye, *Bioorg. Med. Chem. Lett.,* 2014, **24**, 5070–5075.
18. R. Karwal, T. Garg, G. Rath and T.S. Markandeywar, *Ther. Drug Carrier Syst.,* 2016, **33**, 1–39.
19. Y. Wei, J. Zhang, Y. Zhou, W. Bei, Y. Li, Q. Yuan and H. Liang, *Carbohydr. Polym.,* 2017, **159**, 152-160.
20. M. Gallo, A. Favilla and D.G. Mitnik, *Chem. Phys. Lett.* 2007, **447**, 105-109.
21. N. Saikia and R.C. Deka. *Chem. Phys. Lett.* 2010, **500**, 65–70.
22. N Saikia, S Rajkhowa, R.C. Deka. RSC Advances 2016, **6**, 94651-94660.
23. D. Kumar,Y. Krishnan, M. Paranjothy and S. Pal*, J. Phys. Chem. B,* 2017, **121**, 2864-2872.
24. N. Qiu, X. Zhao, Q. Liu, B. Shen, J. Liu, X. Li and L. An, *J. Mol. Liq.,* 2019, **289**, 111151- 111161.
25. S. Gao, C. Bie, Q. Ji, H. Ling, C. Li, Y. Fu, L. Zhao, and F. Ye, *RSC Adv.,* 2019*,* **9**, 26109–26115.
26. S. Mohandoss, R. Atchudan, T. N. Jebakumar, I. Edison, T. K. Mandal, S. Palanisamy, S. G. You, A. A. Napoleon, J. Shim and Y. R. Lee, *Carbohydr. Polym.,* 2019, **224***,* 115166-115176.
27. G. Liu, Q. Yuan, G. Hollett, W. Zhao, Y. Kang and J. Wu, *Polym. Chem.*, 2018, **9**(25), 3436–3449.
28. S. V. Kurkov and T. Loftsson, *Int. J. Pharm.*, 2013*,* **453,** 167–180.
29. Z. Ren, Y. Xu, Z. Lu, Z. Wang, C. Chen, Y. Guo, X. Shi, F. Li, J. Yang and Y. Zheng, *RSC Adv.,* 2019, **9**, 11396–11405.
30. V. B. Chaudhary and J. K. Patel, *Int. J. Pharm. Sci. Res.*, 2013, **4**(1), 68-76.
31. T. Higuchi and K. A. Connors, Phase Solubility Techniques, *Wiley Interscience*, New York, 1965.
32. M. F. Sanner, *J. Mol. Graph. Model.* 1999*,* **17**, 57-61.
33. M. D. Hanwell, D. E. Curtis, D. C. Lonie, T. Vandermeersch, E. Zurek and G. R. Hutchison, *J. Cheminformatics.,* 2012, **4***,* 1-17.
34. Dassault Systèmes BIOVIA, Discovery Studio Modeling Environment, Release 2017, San Diego: Dassault Systèmes, 2016.
35. G. M.Morris, R. Huey, W. Lindstrom, M. F. Sanner, R. K. Belew, D. S. Goodsell, and A. J. Olson, *J. Comput. Chem.,* 2009, **16**, 2785-91.
36. E. F. Pettersen, T. D. Goddard, C. C. Huang, G. S. Couch, D. M. Greenblatt, E. C. Meng and T. E. Ferrin, *J. Comput. Chem.,* 2004, **25**(13), 1605-1612.
37. W. R. Jacobs, R. G. Jr, Barletta, R. Udani, J. Chan, G. Kalkut, G. Sosne, G.J. Kieser, G.F. Hatfull, and B.R. Bloom, *Science,* 1993, **260**, 819–822.
38. V. N. A. Dusthackeer, S. Balaji, N. S. Gomathi, N. Selvakumar and V. Kumar, *Clin. Microbiol. Infect.*, 2012, **18**, 492–496.
39. V.B. Makane, V.S. Krishna, E.V. Krishna, M. Shukla, B. Mahizhaveni, S. Misra, S. Chopra, D. Sriram, V.N.A. Dusthackeer and H.B. Rode, *Eur. J. Med. Chem*., 2019, **164**, 665-677.
40. L. B. Talarico, R. G. Zibetti, P. C. Faria, L. A. Scolaro, M. E. Duarte, M. D. Nosed, C.A. Pujol, E.B. Damonte, *Int. J. Biol. Macromol*, 2004, **34**, 63-71.
41. S. Tanwar, C. Barbey and N. Dupont, *Carbohydr. Polym*., 2019, 217, 26-34.

42. L. Hu, H. Zhang, W. Song, D. Gu and Q. Hu, *Carbohydr. Polym.*, 2012, **90**, 1719–1724.
43. S. A. Razak, S. F. Yaacob, J. M. Abdullah and R. Adnan, *J. Chem. Pharm. Res.,* 2014, **6**(11), 291-299.
44. D. Kuriakose, A. A. Aravindakshan and M. R. P. Kurup, *Polyhedron,* 2017, **127,** 84-96.
45. L. Tom, N. Aiswarya, S.S. Sreejith and M. R. P. Kurup, *Inorg. Chim. Acta,* 2018, **473**, 223–235.
46. L.X. Ding, J.A. He, L.Z. Huang and R.H. Lu, *J. Mol. Struct.,* 2010*,* **979**, 122–127.
47. L.J. Yang, B. Yang, W. Chen, R. Huang, S.J. Yan, J. Lin, *J. Agr. Food Chem.,* 2010, **58**, 8545–8552.
48. M. G. Teixeira, J. V. De Assis, C. G. P. Soares, M. F. Venancio, J. F. Lopes, C. S. Nascimento Jr., C. P. A. Anconi, G. S. L. Carvalho, C. S. Lourenco, M. V. De Almeida, S. A. Fernandes and W.B. De Almeida, *J. Phy. Chem. B*, 2014, **118**(1), 81-93.
49. C. R. Nirmal, N. R. Rao and W. Hopper, *Eur. J. Med. Chem.,* 2015, **105**, 182-93.
50. G. Yalcin, S. Burmaoglu, I. Yildiz and O. Algul, *J. Mol. Struct.,* 2018, **1164**, 50-56.
51. N.C. Desai, A.R. Trivedi and V.M. Khedkar, *Bioorg. Med. Chem. Lett.,* 2016*,* **26**, 4030–4035.
52. K. Mikusová, V. Makarov and J. Neres, *Curr. Pharm.,* 2014*,* **20**(27), 4379-4403.
53. R. V. Chikhale, M.A. Barmade, P.R. Murumkar and M.R. Yadav, *J. Med. Chem.,* 2018*,* **61** (19), 8563-8593.
54. S.V. Calenbergh, S. Pochet and H. Munier-Lehmann, *Curr. Top. Med. Chem.,* 2012, **12**, 694-705.
55. A. Vijayalakshmi, V. Ravichandiran, S. Jayakumari, A. Selvakannan and G. Sangeetha, *Der Pharma Chem.,* 2016, **8**(19), 249-256.
56. D. Lopes-de-Campos, R.M. Pinto, S.A. Lima, T. Santos, B. Sarmento, C. Nunes and S. Reis, *Int. J. Nanomedicine,* 2019, **14**, 2781–2795.

View Article Online
DOI: 10.1039/C9NJ06351J

Formulation and Evaluation of *β*-Cyclodextrin-mediated Inclusion Complexes of Isoniazid Scaffolds: Molecular Docking and *In Vitro* Assessment of Antitubercular Properties

Lincy Tom[a]*, Christy Rosaline Nirmal[b], Azger Dusthackeer[b], B. Mahizhaveni[b] and M.R. Prathapachandra Kurup[a,c]

Inclusion complexes of isoniazid derivatives with *β*-CD were synthesized and their potent anti-tubercular properties were studied.

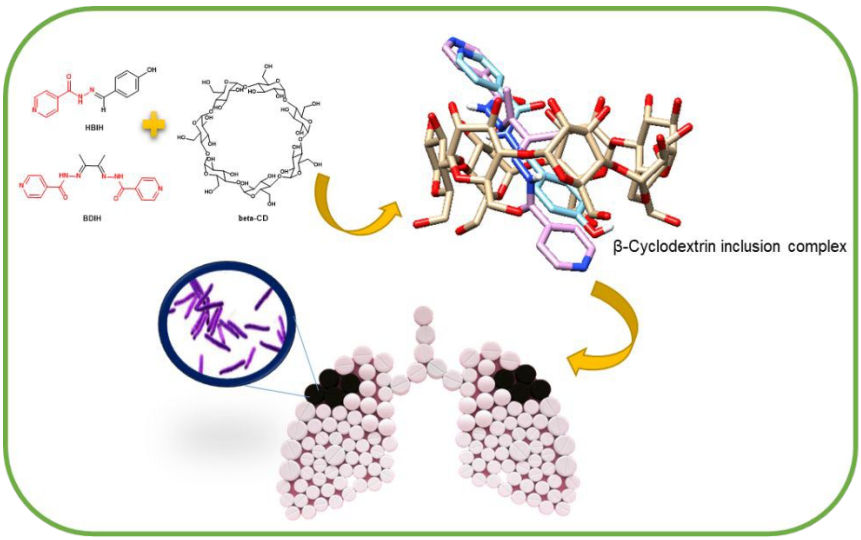

View Article Online
DOI: 10.1039/C9NJ06351J